# Effect of envelope characteristics on the accuracy of discretised greenhouse model in TRNSYS

Qazeem Opeyemi Ogunlowo,[1,2] Wook Ho Na,[3] Anis Rabiu,[1] Misbaudeen Aderemi Adesanya,[1] Timothy Denen Akpenpuun,[4] Hyeon Tae Kim,[5] Hyun Woo Lee[1,3]

[1]Department of Agricultural Civil Engineering, College of Agricultural and Life Sciences, Kyungpook National University, Daegu, Korea; [2]Department of Agricultural and Bioenvironmental Engineering, Federal College of Agriculture Ibadan, Ibadan, Nigeria; [3]Smart Agriculture Innovation Centre, Kyungpook National University, Daegu, Korea; [4]Department of Agricultural and Biosystems Engineering, University of Ilorin, Ilorin, Nigeria; [5]Department of Bio-Industrial Machinery Engineering, Gyeongsang National University, Jinju, Korea

## Abstract

TRNSYS is a standard tool recently used to model and simulate greenhouse energy demand and utilisation using building energy simulation (BES). Previously, a single thermal point was used for validation, ignoring the distribution of greenhouse climate parameters, especially the temperature. Temperature variation often leads to thermal stratification, prompting researchers to propose volume discretisation in dynamic greenhouse simulations. In this context, the effect of envelope characterisation on the accuracy of the discretised TRNSYS BES model was developed to determine the best BES model under a free-floating regime. The combination of the number of layers [double (D) and single (S)], geometry mode [3D and manual (M)], and layer type [massless (M) and no glazing window (W)], led to the development of five models: D_3D_M, D_3D_W, D_M_M, S_3D_W, and S_M_M. The simulation was performed in a standard radiation mode, and the output parameters were temperature and relative humidity (RH). $R^2$ and the root square mean error (RSME) were used to check the fitness and degree of deviation, respectively, to validate the models. Analysis of variance (ANOVA) was employed to investigate the significant differences among the models, whereas contour plots were used to compare the distribution pattern between the significant models and experimental data. Validation of the models showed that the obtained $R^2$ values ranged from 0.86 to 0.95, and the RSME values for the temperature were between 2.64°C and 3.91°C. These values were 0.91-0.93 and 19.72%-30.32% for RH. The ANOVA (P<0.05) result exhibited significant differences between the S-scenario models and experimental central points in temperature and RH. However, the D- and S-layer scenarios with a 3D geometry and massless layer showed similar distribution with their corresponding experimental greenhouses. Hence, 3D_M was regarded as the best combination in the discretised BES model.

## Introduction

The greenhouse is an agricultural structure built to shield plants from harsh ambient climate. These structures are often covered (enveloped) to allow passage of sunlight, retain heat during winter or cold days, and allow ventilation during summer. Greenhouse practices are aimed at achieving optimum microclimate conditions for plant growth or yield, and energy is often added or removed to ensure that the microclimate parameters such as temperature, relative humidity (RH), solar radiation (SR), carbon dioxide ($CO_2$), and vapour pressure deficit (VPD) are optimum. The enveloping material can be characterised based on the material type, property, and the number of layers. Depending on the type of greenhouse (single- or multi-span type), the covering

material can be polyolefin (PO), polyethylene (PE), glass, or polycarbonate (PC). PO and PE usually cover single-span greenhouses, whereas glass and PC are used in Venlo-type multi-span greenhouses (Shamshiri, 2007). Several researchers recently, such as Rabiu *et al.* (2022), have determined the thermophysical, radiative, and aerodynamic properties of selected commercial greenhouse thermal screens. To decide on their respective U-values as the U-value is essential in the selection of an appropriate covering or thermal screen materials. In particular, Rafiq *et al.* (2019) developed a new radiation balance method for determining emissive power, absorptive capacity, reflectivity, transmissivity, and emissivity of entirely or partially transparency materials using pyrgeometer and net radiometer. While Rafiq *et al.* (2021) modified the radiation balance methods for determining the total hemispherical longwave radiative properties of screen materials with zero porosity, partially opaque, and asymmetric screens using wide-band radiometers. Unlike Rafiq *et al.* (2019) and Rafiq *et al.* (2021) Rasheed *et al.* (2017) investigated the transmissivity, absorption, heat conservation, and transmission of selected covering materials. The findings from these researches have been subsequently used to define the respective material properties in TRNSYS. The need to increase the heat-retaining efficiency of single-layer greenhouses (SLGs) has led to the development of two-layer-covered greenhouses, also known as double-layer greenhouses (DLGs). Akpenpuun *et al.* (2021a) observed that the double-layer conserved more energy by approximately 58.2% than the single-layer.

Transient system simulation (TRNSYS) is a building energy simulation (BES) program, a multifaceted component-based software capable of dynamically simulating simple and complex energy systems in buildings. The TRNSYS software consists of an engine that processes input files and a component library (Klein, 2012; Akpenpuun *et al.*, 2022). TRNSYS is a product of the University of Wisconsin's Solar Energy Laboratory and was developed, released, and commercialised in 1975 (Klein, 2012; Akpenpuun *et al.*, 2022). Standard BES tools include computational fluid dynamics (CFD), EnergyPlus, and TRNSYS.

BES is an instantaneous energy demand technique based on various dynamic simulation procedures that forecast and analyse energy (Akpenpuun *et al.*, 2022). A virtual greenhouse-structure BES model can be developed to receive weather data, properties of the envelope materials, and energy as output.

Rasheed *et al.* (2020) successfully developed and validated a building energy simulation model to investigate the effect of different thermal screens, natural ventilation, and heating setpoint controls on annual and maximum heating loads of a multi-span greenhouse. While Mazzeo *et al.* (2020) developed a BES model to evaluate the prediction accuracy of building performance simulation (BPS) tools, namely TRNSYS, EnergyPlus and IDA ICE and successfully validated their model with experimental measurements under actual operating conditions. Boulard *et al.*, 2008 and Asa'd *et al.*, 2019 on the other hand, developed BES models that successfully simulated the dynamic influence of the insect screens and tomato crop on airflow movement, using the concept of the porous medium and investigated the efficiency of a rock-bed thermal storage heating system of an attached solar greenhouse, respectively.

Choab *et al.* (2021), Rasheed *et al.* (2018, 2019), and Ward *et al.* (2015) also used TRNSYS to model the greenhouse energy demand successfully by comparing the mean indoor and ambient temperatures. Although they collected data from multiple points in experimental greenhouses, only a single thermal point/node was considered in the building simulation. Studies have shown that significant variation exists in the distribution of greenhouse microcli-

mate parameters such as temperature, RH, SR, $CO_2$, and VPD along the vertical axis (Cesar *et al.*, 2021; Lamrani *et al.*, 2001; Zhao *et al.*, 2001) and horizontal dimensions in greenhouses despite the installation of distribution fans (Ogunlowo *et al.*, 2021). According to Baglivo *et al.* (2020), this variation leads to thermal stratification, which affects the natural-ventilation control and demonstrates that volume discretisation is an essential feature in a dynamic greenhouse simulation.

Discretisation is a technique that transforms continuous attributes, variables, models, or functions into discrete ones (Gupta, 2019). This technique allows the distribution of microclimate parameters in BES, as demonstrated in experimental greenhouses. Among the standard BES tools, CFD provides vertical and horizontal stratification/discretisation functions predefined in its operation, hence its potential for parameter distribution. TRNSYS is another tool with features for discretisation, although it is seldom used (Baglivo *et al.*, 2020). According to TRANSSOLAR Energietechnik (2017), the TRNSYS thermal point is called an 'air node', and simulation of multi-air node zones is an advanced modelling feature. Large volumes, such as in atria, are often modelled using a stack of air nodes within one zone. Thus, the top air node may have a higher temperature than the bottom air node. However, SR that enters a zone is distributed to all surfaces of all air nodes in this zone. Therefore, the radiation transmitted by the roof glazing of the top air node can fall on the floor surface of the bottom air node (TRANSSOLAR Energietechnik, 2017). In contrast to CFD and EnergyPlus, TRNSYS is known for its flexibility because it allows the introduction of new models that can be linked together. Model accuracy is measured via model validation or verification. To validate a model, the following indexes, namely, *R* squared ($R^2$), mean absolute error (MAE), root square mean error (RSME), and Nash-Sutcliffe efficiency, have been used over the years (Asa'd *et al.*, 2019; Rasheed *et al.*, 2018; Villagrán *et al.*, 2019). In the words of Glen (2019), '*Model evaluation techniques answer three main questions: How well does your model match your data (in other words, what is the goodness of the fit? Assuming you have created multiple models, which one is the best? Will your model predict new observations for your data set with accuracy?*' $R^2$ measures how well the model fits, *i.e.*, how well two data sets fit each other. In addition, it determines whether the trend is similar or different. RSME and MAE measure the deviation in the data sets. They indicate the robustness of the data around the line of best fit. According to Hamad *et al.* (2008), the graphical model-validation methods could display the model and simulation data to complement the validation statistics such as RSME. According to Blachowski (2021), although often overlooked, model calibration is important because it provides insight into the model uncertainty, which can later be used for further processing of the model outputs. As stated by Coastalwiki (2020), '*Model calibration is the process of adjustment of the model parameters and forcing within the margins of the uncertainties (in model parameters and/or model forcing) to obtain a model representation of the processes of interest that-satisfies pre-agreed criteria-observation (goodness-of-fit or cost function).*'

Regression is often used in model-calibration methods, as verified by Blachowski (2021), Sanft and Walter (2020), and Sunmin (2021).

In a recent study, a discretised greenhouse TRNSYS-based BES model was developed by Baglivo *et al.* (2020) to simultaneously simulate the dense-volume discretisation, 3D shortwave- and longwave-radiative exchanges, airflow exchanges, 3D positioning of lamps, ground, plant evapotranspiration, and convective heat transfer coefficients. According to Baglivo *et al.* (2020), there are

three different options for thermal zone separation, as illustrated in Figure A1. To realise discretisation, adjacent walls were defined as Virtual windows. They claimed Virtual window should be best used as it allows heat transfer and solar radiation is treated accurately by separating the beam component from the diffuse one. Unlike the Massless layer, which only allows thermal transfer through walls, the Virtual surface only allows solar transfer. However, the claim appeared to be a mere assertion rather than an experimental fact because no reference supported the claim. In addition, because TRNSYS 17 was used, the version suffered from the limitations of surface definition. This model was, however, not validated with experimental data but by an EnergyPlus validated model developed by Mazzeo *et al*. (2020).

The need for a discretised BES model cannot be overemphasised as Baglivo *et al.* (2020) have suggested a need for a model that considers the horizontal and vertical distribution to accurately evaluate the energy requirements in the greenhouse. A 32% reduction in the annual energy needs of the large building was reported by Laghmich *et al*. (2022) when horizontal distribution was considered compared to a single thermal point model. Both Baglivo *et al.* (2020) and Laghmich *et al.* (2022) used TRNSYS 17 to develop their discretised BES model, and as earlier mentioned, it has its limitations. Energy and mass exchanges occur between the greenhouse microclimate and ambient environment, and the use of TRNSYS 18 to create a discrete BES model has not been reported nor identifying the best use of the envelope characters in this version. Therefore, creating a model that accurately mimics the transfer across the external and adjacent air node envelopes and shows the distribution within the greenhouse interior is necessary. To create a more accurate discretised BES model in TRNSYS 18 (the latest version), there is a need to select the model with the best envelope characters. Hence, studying the effect of the envelope characteristics defined in TRNSYS 18 on the model accuracy is essential. In this context, the objectives of the present study are to develop discretised BES models based on the envelope characteristics defined in TRNSYS 18 and to determine which model best mimics the experimental greenhouse scenario under a free-floating regime.

## Materials and methods

To develop a BES model in TRNSYS 18 - transient systems simulation tool, a commercial software package designed at the University of Wisconsin, tools such as SketchUp, TRNBuild, and Window 7.4 are needed. The greenhouse structure is represented by a Type-56 component in the TRNSYS simulation studio. For it to function, a detailed building description is required in a .*bui* (*dot bui*) format, which can be achieved using TRNBuild - a TRNSYS tool for building description. In addition, the building's envelope characteristics and regime (geometry of the buildings, radiation mode, infiltration and ventilation, number of zones/air nodes, and thermal and moisture capacitance of the zone/air node) are required by the building defined in TRNBuild. The greenhouse geometry can be defined manually in TRNBuild or imported as an .*idf* file format in SketchUp 2017. SketchUp is a building 3D software developed by Trimble incorporation.

### Envelope characteristics in TRNBuild

#### *Zone-air node in TRNBuild*

When a Trnsys3d file (.*idf*) is imported into TRNBuild from SketchUp, zones and geometry are automatically created. In addition, the geometry mode is automatically set to 3D data, thus, a 3D geometry. In this mode, the data cannot be modified.

To manually add a new zone, also known as manual mode, the zone icon in the TRNBuild navigator is used. The number and name of the zones and air nodes can be added, whereas the zone dialog box that contains all the information that describes the thermal zone of the building is opened.

Generally, a zone consists of one air node, but the simulation of multi-air node zones can also be a possible feature. To create the discretised model shown in Figure A2(A), the zones are stacked, whereas air nodes are stacked within each zone, as shown in Figure A2(B). In the standard mode, SR that enters a zone is distributed to all surfaces in all air nodes in that zone. Thus, the radiation transmitted by the roof glazing of the top air node can fall on the floor surface of the bottom air node. In addition, all surfaces of every air node in a zone undergo a longwave-radiation exchange when the detailed longwave-radiation mode is used. The data describing an air node can be divided into four main parts, as in Table 1.

- *Required regime data* - These data are entered into the regime-data section in each air node, as listed in Table 2: i) *volume*: volume of air in the air node; ii) *capacitance*: total thermal capac-

**Table 1. Categorisation of air node envelope characters in TRNbuild.**

| Air node envelope characterisation | Category |
|---|---|
| Required regime data | i. Volume<br>ii. Capacitance<br>iii. Reference floor area |
| Opaque surfaces | i. External<br>ii. Internal<br>iii. Adjacent<br>iv. Boundary |
| Layer type | Massive<br>Massless |
| Windows | i. External<br>ii. Adjacent |
| Optional regime | i. Free-float (no heating or cooling)<br>ii. Coupling<br>iii. Infiltration<br>iv. No ventilation |

itance of the air node air plus that of any mass not considered as walls (*e.g.*, plant bed, irrigation tank, and boiler); iii) *reference floor area*: reference floor area of the air node.

*- Opaque surfaces of the air node -* The surface category is set to EXTERNAL by default. The following surface categories are available, as shown in Figures A3 and A4: i) EXTERNAL: an exterior surface; ii) INTERNAL: a surface of an air node; iii) ADJACENT: a surface that borders another air node; iv) BOUNDARY: a surface with boundary conditions.

For the definition of a surface layer, two out of four available options are considered: i) *massive*: the most common option usually used in all constructions; ii) *massless*: this option is only used when TRNBuild cannot create the transfer functions of a wall using only the massive layers. In this case, the layer type is used for very thin layers where the thermal mass can be neglected. Table 3 lists the properties of the opaque surfaces in this study.

*- Windows of the air node -* Windows can be defined as external and adjacent opaque surfaces or as an additional window without a related base surface. The windows have a unique ID number identifying the connection to the glazing system's optical and thermal property data. These properties are generated by the Window 7.4 software developed by Lawrence Berkeley National Laboratory (LBNL). For the window, we can also choose 'no glazing', in which the surface is imaginary. Table 3 lists the glazing-material properties used to generate the properties in Windows 7.4 software.

*- Optional regime:* i) in this study, the heat source simply comes from SR. Hence, the system is in a free-floating regime; ii)

regime coupling enables coupling of the air nodes of adjacent surfaces. Up to six coupling airflows from 'adjacent' air nodes can be defined in each air node. The coupling is first activated, and the air node from which the airflow originates is then selected. Finally, the coupled airflow is defined as a constant (0 m/s), indicating a fully closed greenhouse condition.

iii. Infiltration is defined as the introduction of ambient air into the building through cracks in the construction due to the pressure difference between the inside of the greenhouse and the ambient. The infiltration is set to a constant value of 10.0 air-change hour for the entire greenhouse and a fraction of the air node volumes for each air node in the simulation.

### Convection coefficients

The convection coefficients for heat transfer from the exterior of the building to the greenhouse microclimate depend on the ambient condition. Therefore, we need to define the input using a value. Eq. 1 defines the value of heat convection in this study:

$$h_{ext}\left(\frac{kJ}{hm^2K}\right) = 3.6 \times (3.8W_s + 7.4) \tag{1}$$

where $h_{ext}$ and $W_s$ are the heat-convection coefficient and external wind speed, respectively. A new equation block named convection is added to add this calculation to the simulation process. The wind speed and exterior convection coefficient are input and output variables. From the definition of the equation block, the wind speed is

**Table 2. Regime definition of the air nodes.**

| Area | Air node/Zone | Volume (m³) | | Capacitance (kJ/K) | | Ref. floor area (m²) |
| --- | --- | --- | --- | --- | --- | --- |
| | | Single | Double | Single | Double | |
| Floor | F1-9 | 13.01 | | 77.98 | | 13.01 |
| Crop | A-E | 8.45 | | 50.69 | | 13.01 |
| Canopy | Ca1-3, Ca7-9 | 11.98 | | 21.56 | | 13.01 |
| | Ca4-6 | 20.73 | | 24.88 | | 13.01 |
| Roof | R1-3, R7-9 | 9.53 | | 11.43 | | 17.56 |
| | R4-6 | 15.26 | 14.96 | 91.54 | 89.74 | 13.01 |
| Corridor | Co1-6 | 2.48 | | 2.97 | | 1.50 |
| West end | West | 124.33 | 123.33 | 745.99 | 739.99 | 35.00 |
| East end | East | 24.87 | 24.67 | 29.84 | 29.60 | 7.00 |

**Table 3. Material properties as defined in TRNBuild.**

| Surface type | Category | Material | Thickness (m) | U-Value (W/m²K) | Layer type |
| --- | --- | --- | --- | --- | --- |
| Opaque | Ext-wall/roof | Steel | 0.05 | 5.769 | Massive |
| | Adj-wall1 | PO-MW-PO composite | 0.05 | 0.999 | Massive |
| | Adj-wall2/ceiling | Steel | 0.04 | 5.792 | Massive |
| | Adj-wall3 | Air layer | 0.00 | 2.948 | Massless |
| | Boundary | Ground floor | 0.10 | 2.611 | Massive |
| Glazing | Ext-window | PO | ST (0.86)*, SR (0.10)*, VRT (0.89)*, VRR (0.08)*, TRT (0.18)*, TRE (0.79)*, TC (0.33)*, T (0.10)* | | |
| | Adj-window1 | | | | |
| | Adj-window2 | 'No glazing' | 0.00 | 5.680 | Massless |

*Properties used in Window 7.4 LBNL (Source: Rasheed *et al.*, 2020). Ext, external; Adj, adjacent; PO, polyolefin; MW, mineral wool; ST, solar transmittance; SR, solar reflectance; VRT, visible radiation transmittance; VRR, visible radiation reflectance; TRT, thermal radiation transmittance; TRE, thermal radiation emission; TC, thermal conductivity (W/mK); T, thickness (mm).

connected from the weather-data type to the equation block, and the convection coefficient is connected from the equation block to the building component.

## Balance outputs in TRNBuild

### Solar balance for the zones (Ntype 901)

According to TRANSSOLAR Energietechnik (2017), solar balance indicates how much SR is blocked, how much enters the zone, and how much is exchanged with the other zones. This balance is printed for all zones in one file when NType 901 is selected in the output manager for one zone. For a massless layer or in the absence of a glazing window, *i.e.*, no external window, shading, or absorbed solar gains in the window or wall, the solar balance is expressed by Eq. 2:

$$Q_{BAL}(kJ/h) = Q_{SOLAIR} \pm Q_{SADJ} \qquad (2)$$

where $Q_{BAL}$ is the solar balance for one zone to approach zero and $Q_{SADJ}$ represents the solar gains due to the exchange with adjacent zones (gains: +; losses: −), including multiple reflections. $Q_{SOLAIR}$ is the convective-energy gain of the zone due to transmitted SR through the external windows, which is immediately transformed from a convective heat flow into internal air.

### Moisture balance in the zones (Ntype 907)

According to TRANSSOLAR Energietechnik (2017), this balance indicates the moisture balance in all separate zones. We must note that the humidity ratio reaches 100% with a positive water gain to the zone. The positive water gain increases the amount of water stored in the air, eventually forming water droplets on the cladding surfaces. For a massless layer without a surface for water storage, ventilation, water gains due to internal loads, and water gain or loss through humidification and dehumidification, the moisture balance equation is expressed as follows:

$$MW_{BAL} = MDW_{AIR} - MW_{INF} - MW_{COUP} \qquad (3)$$

where:
$MW_{BAL}$ is the moisture balance in each zone should be close to zero;
$MDW_{AIR}$ is the change in the water stored in the air zone;
$MW_{INF}$ is the water gain in the zone due to infiltration;
$MW_{COUP}$ is the water gain in the zone due to coupling.

## Model-development scenarios

Three factors were considered in this study: i) *number of layers*: double (D) and single (S); ii) *geometry mode*: 3D and manual (M); iii) *Adj_Wall3 Layer type*: massless (M) and 'no glazing' window (W).

The combination of these factors led to the development of five models: D_3D_M, D_3D_W, D_M_M, S_3D_W, and S_M_M. The simulation was performed in a standard radiation mode, and the output parameters were the temperature and RH. Figure 1 shows the model component connections in the TRNSYS simulation studio. The weather, building, and output components are shown in orange, yellow, and blue rectangles.

The DLGs and SLGs were built in Daegu, South Korea, located at 35.53°N, 128.36°E, and were 48 m above sea level. Both greenhouses were single-span gothic-type roofs covered with PO and oriented in the east-west direction (71°). The gross volume was 553.1 m$^3$, the floor area was 168 m$^2$, and the dimensions were 24×7×4 m.

For this study, the greenhouses were closed entirely without natural or mechanical ventilation. Nine Hobo onset U23-002 sensors with a sensitivity of ±0.21°C (range 0°C-50°C) and ±2.5% RH (10%-100% RH) were horizontally installed within the crop area to record the air temperature (*T*) and RH. Figure 2 shows the positions of the sensors and dimensions of the model greenhouses shown in Figure A4. All sensors recorded the data every 10 min. The data were collected from August 27, 2021, to September 8, 2021.

## Model validation

$R^2$ and RSME were used to verify whether the trend and degree of deviation fitted, respectively, to validate the models. Analysis of variance (ANOVA) was used to confirm if a significant difference existed among the models; in contrast, a contour plot was used to
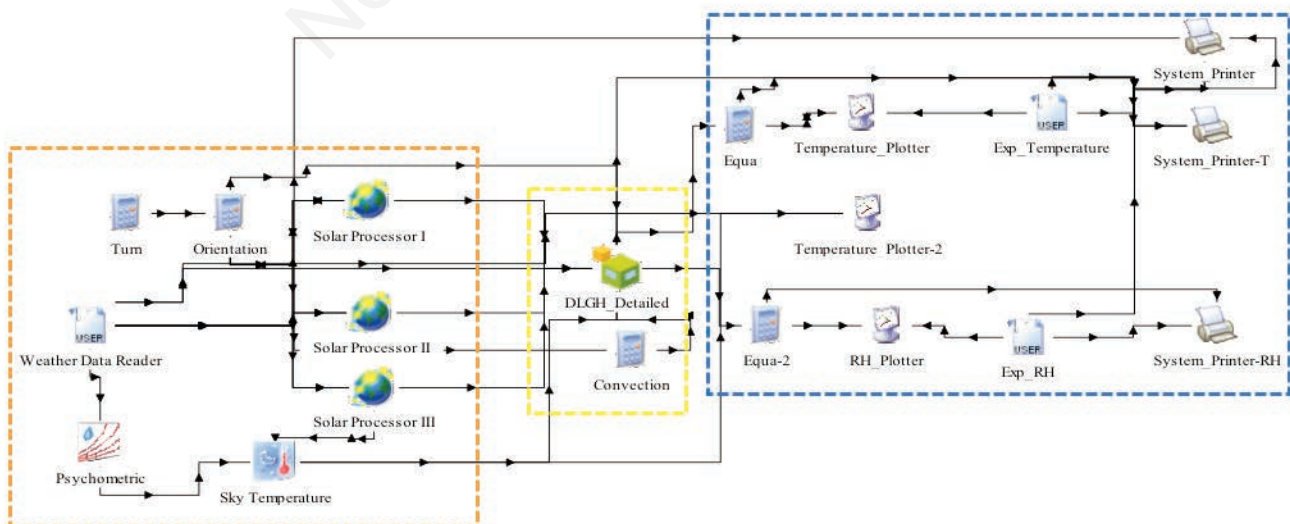


**Figure 1. Greenhouse-model representation in TRNSYS simulation studio 18.**

compare the distribution pattern between the significant models and experimental data. A similar ANOVA equation (Eq. 4) and the hypothesis used by Ogunlowo and Olaoye (2017) were adopted.

$$Y_{ijl} = \mu + a_i + b_j + ab_{ij} + e_{ijl} \qquad (4)$$

where $Y_{ijl}$ represents the $l$th observation due to treatments $i$ and $j$, μ represents the overall means, represents the effect of treatment $i$, $b_j$ represents the effect of treatment $j$, $ab_{ij}$ represents the effect of the interaction, and $e_{ijl}$ is a random term.

The ANOVA hypothesis is as stated below:

Null hypothesis $H_{01}$: the effects of factor combination are the same, i.e., $a_1 = a_2 \ldots = a_{n=} 0$.

Alternative hypothesis $H_{11}$: the effect is not the same, i.e., $a_1 \neq 0$.

Decisions: If $F < F_{crit}$, then $H_{01}$ should not be rejected; otherwise, $H_{11}$ is accepted.

Microsoft Excel 2019 ($R^2$, RSME, and ANOVA) and Surfer 13 (contour plot) were used.

## Results and discussion

Three double-layer and two single-layer scenarios were modelled as presented in the *Materials and methods* section. Figures 3 and 4 compare the simulated and experimental temperature and RH results in the D and S scenarios. Figure 2 shows that during the day, the M_M simulated temperature trend was similar to the experimental temperature, whereas the trend at night was dissimilar. The 3D_W trend was the least during the day but was more than the M_M trend and lower than the 3D_M trend. The 3D_M trend was better at night but fell within the M_M and 3D_W trends during the day. However, a reverse case was observed for RH. In the S-scenario, Figure 4 shows that the temperature trend of 3D_M was below the experimental result during the day but more than that at night. The trend was lower for M_M both during the day and night. A reverse was observed for RH.

Figures 5 and 6 show a one-on-one plot of the day and night simulated temperature and RH values against the experimental value for the D and S scenarios, respectively. Figures 5A and 6A show a logarithmic curve fit between the simulated and experimental temperature, whereas the RH demonstrated a polynomial curve fit (Figures 5B and 6B).

The $R^2$ and RSME values of the temperature indicated a good fit between the D-scenario models and the experimental trend, where the M_M model exhibited the highest $R^2$ value of 0.95 and the 3D_W model showed the lowest value of 0.90. Meanwhile, the RSME value was the lowest in the M_M model (2.64°C) and the highest in the 3D_W model (3.75°C). The ANOVA of the temperature indicated that no significant difference existed between the models and experimental data. The models fit the simulated and experimental RH trend. The $R^2$ ranking of RH ranged from 0.93 in the M_M model to 0.91 in the 3D_W model. However, the RSME value was the lowest for the 3D_W model (28.02%) and the highest for the 3D_M model (30.32%). These results indicated that the trends fitted well. A deviation of approximately 28%-30% in RH existed between the models and experimental value. RH's ANOVA result showed a significant difference between the D-scenario models and the experimental trend. However, no significant differ-
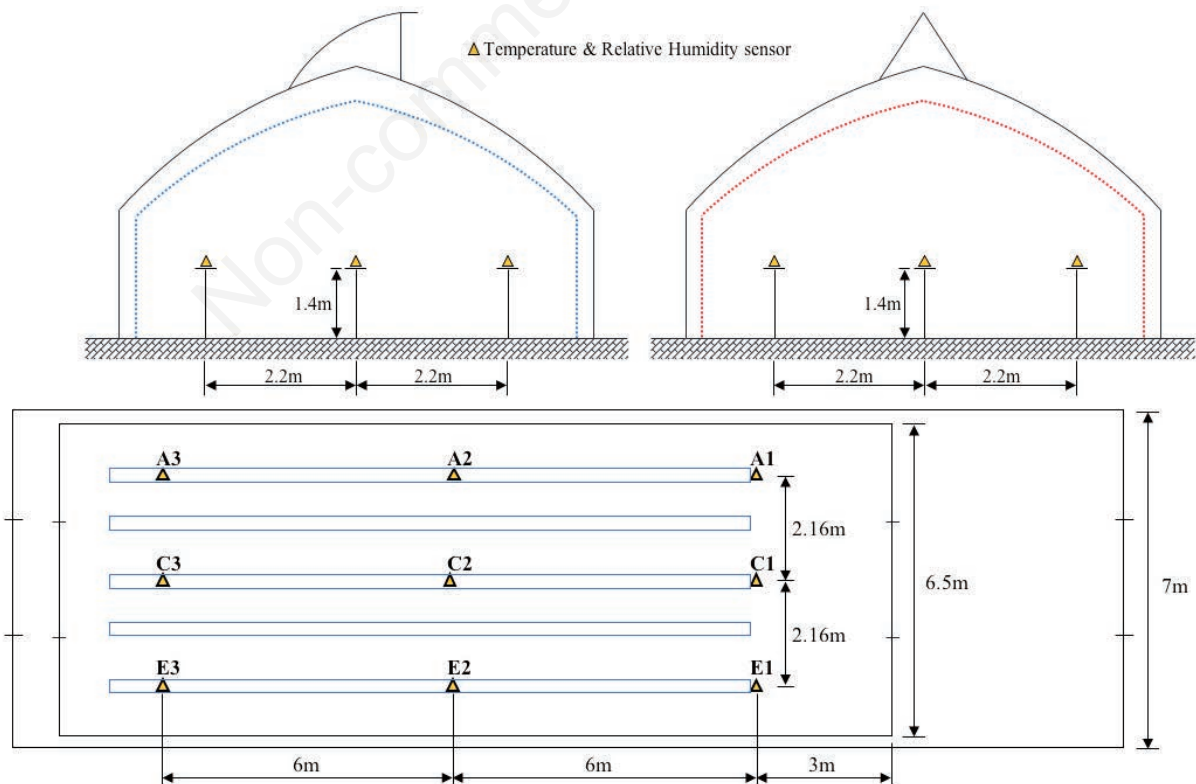


**Figure 2. Crop-area sensors located in double-layer greenhouses and single-layer greenhouses.**

ence existed between the three models. For the S-scenario models, the $R^2$ trend of the temperature demonstrated a good fit between the models and the experimental data. The 3D_M model exhibited the highest $R^2$ value of 0.88, whereas M_M had the lowest $R^2$ value of 0.86. However, the RH trend demonstrated a better fit for the 3D_M (0.93) and M_M (0.92) models. On the other hand, the RSME values of the temperature were 2.81°C and 3.91°C for the 3D_M and M_M models, respectively, whereas the RH values were 28.41% and 19.72% for the same models. The ANOVA result indicated a significant difference between the S-scenario models and the experimental trend.

During the day, because the models were developed under a free-floating regime, the air node/zone heating simply originated from SR through the external windows and upper stacked air nodes. This condition implied that the temperature of the centre air node in both the D and S scenarios was obtained through the solar gains due to the exchange with adjacent zones or air nodes and the convective-energy gain of the zone (Eq. 2). This result was made possible because, in the standard mode in TRNSYS, SR through the roof glazing of the top air nodes fell on the floor of the bottom air nodes. This result implied that, in contrast to the claim by

Baglivo *et al*. (2020), TRNSYS 18 allows thermal transfer and radiation through a massless layer, as the U-value influences the models. Table 3 indicates that the U-value of the 'no glazing' window (5.68 W/m$^2$·K) influences $R^2$ and RSME of the 3D_W model, as listed in Table 4. Because the value was higher than that of the massless layer (2.948 W/m$^2$·K), higher heat loss and lower temperature values were realised. Therefore, $R^2$ was low, and RSME was increased compared with those of the massless-layer models.

The high deviation in the D-scenario listed in Table 4 and shown in Figures 2 and 3 could be attributed to the fact that DLGs contained higher RH than the SLGs, as evidenced in the report by Akpenpuun *et al*. (2021a, 2021b) and Ogunlowo *et al*. (2021). From Eq. 3, because the models had no ventilation, the change in RH was due to the water gain through infiltration and coupling from adjacent zones. The model could not account for the presence of the initial moisture in the experimental greenhouses before they were fully closed. Near-crop-area sensors were used to determine which models had a similar distribution to the experimental greenhouse scenarios. Horizontal distribution was considered, and Figures 7 and 8 show the temperature distribution in the D and S scenarios, respectively. Figure 7A and B show similar contour pat-
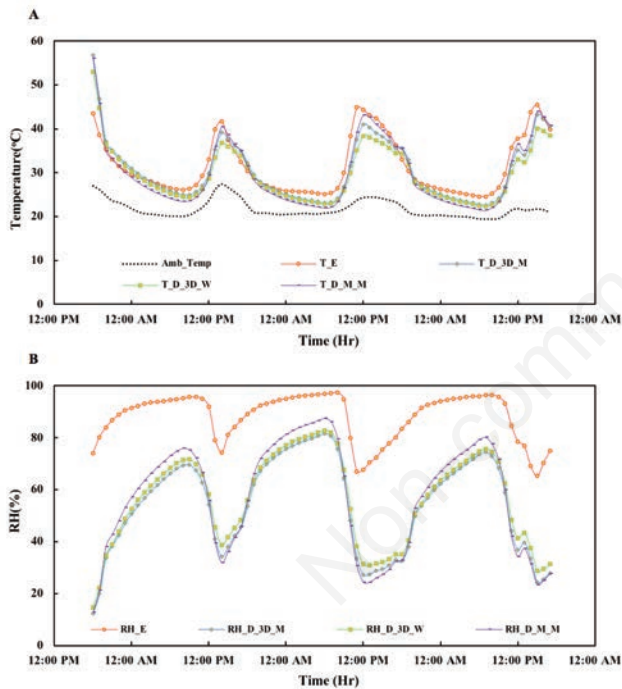


**Figure 3. Comparison of the experimental and simulated results in the D-scenario. A) Temperature; B) relative humidity (RH).**
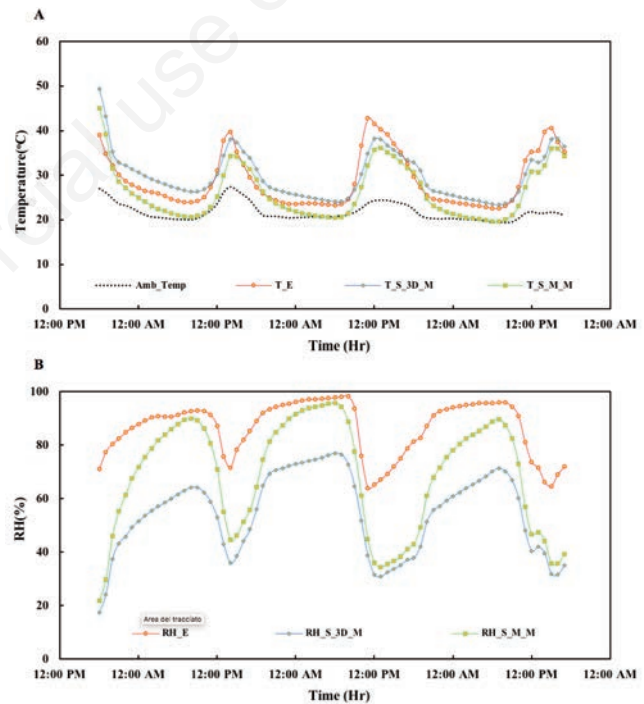


**Figure 4. Comparison of the experimental and simulated results in the S-scenario. A) Temperature; B) relative humidity (RH).**

**Table 4. Validation result of the central thermal node (C2): $R^2$, RSME, and ANOVA.**

| | D | | | S | |
| | 3D_M | 3D_W | M_M | 3D_M | M_M |
|---|---|---|---|---|---|
| $R^2$_T | 0.93[b] | 0.90[c] | 0.95[a] | 0.88[a]** | 0.86[b]** |
| $R^2$_RH | 0.92[b]* | 0.91[c]* | 0.93[a]* | 0.93[a]** | 0.92[b]** |
| RSME_T | 2.74[b] | 3.75[c] | 2.64[a] | 2.81[a]** | 3.91[b]** |
| RSME_RH | 30.32[c]* | 28.02[a]* | 29.50[b]* | 28.41[b]** | 19.72[a]** |

[a,b,c] Rank.*Significance between the experiment and models; **significance between the models and experiment (P<0.05).

**A** T_D_3D_M

$$y = 28{,}2\ln(x) - 67{,}013$$
$$R^2 = 0{,}9394$$

**B** RH_D_3D_M

$$y = 0{,}0631x^2 - 8{,}6192x + 323{,}35$$
$$R^2 = 0{,}967$$

T_D_3D_W

$$y = 24{,}713\ln(x) - 55{,}938$$
$$R^2 = 0{,}9168$$

RH_D_3D_W

$$y = 0{,}0647x^2 - 8{,}9812x + 344{,}36$$
$$R^2 = 0{,}9619$$

T_D_M_M

$$y = 33{,}939\ln(x) - 86{,}903$$
$$R^2 = 0{,}959$$

RH_D_M_M

$$y = 0{,}0697x^2 - 9{,}4061x + 342{,}9$$
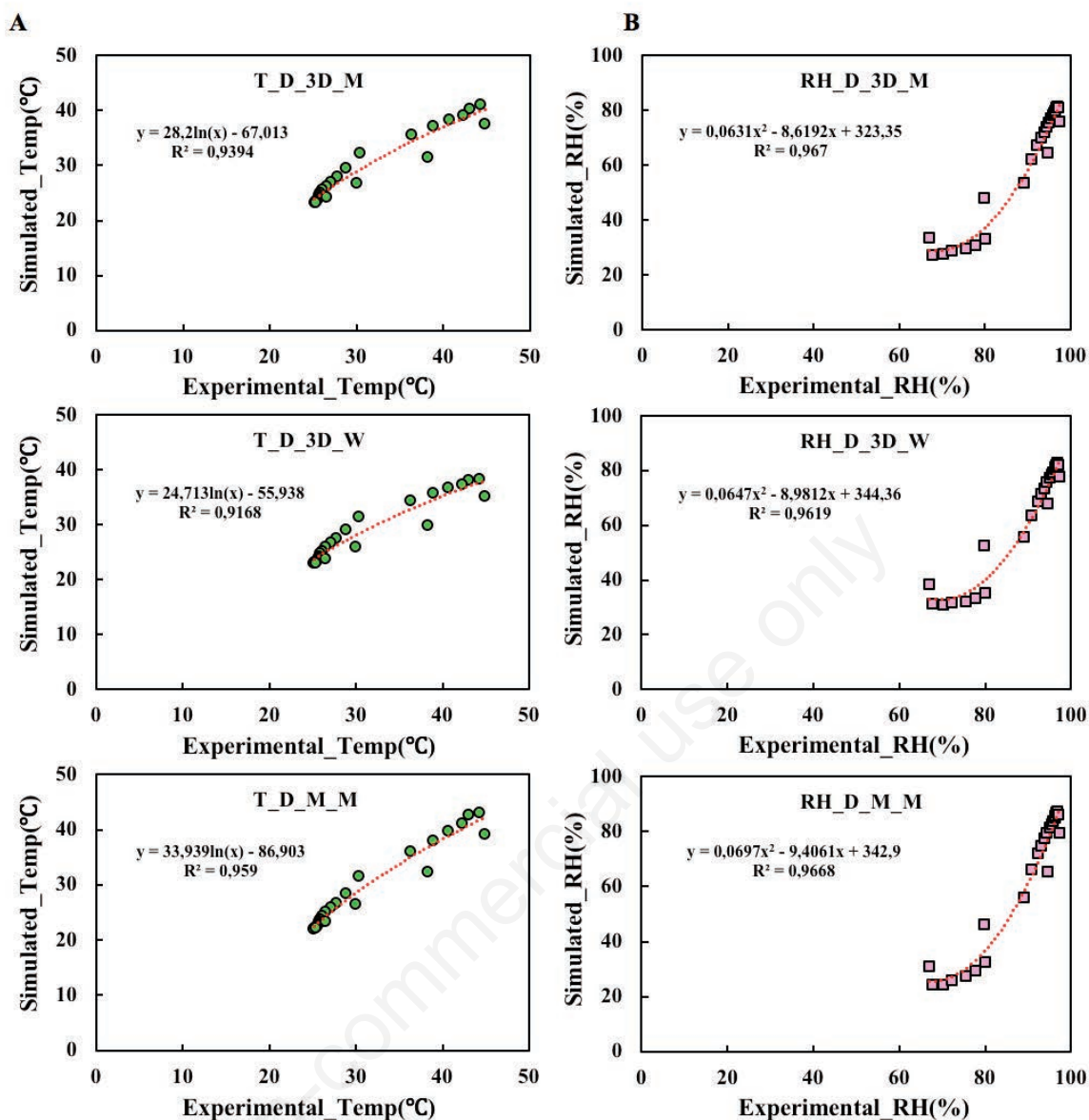$$R^2 = 0{,}9668$$

**Figure 5. Plot of simulated *versus* experimental (A) temperature and (B) relative humidity (RH) in the D-scenario.**

**Table 5. Validation result of the crop-area horizontal thermal-node temperature: $R^2$ and RSME.**

| EXP_VS_SIM | Equation | D_3D_M $R^2$ | RSME | Equation | D_M_M $R^2$ | RSME | Equation | S_3D_M $R^2$ | RSME | Equation | S_M_M $R^2$ | RSME |
|---|---|---|---|---|---|---|---|---|---|---|---|---|
| A1 | y=12.588e0.0297x | 0.94 | 2.01[a] | y=11.307e0.0338x | 0.93 | 2.74[b] | y=10.307e0.0341x | 0.90 | 2.21[a] | y=12.875e0.0325x | 0.90 | 5.19[b] |
| A2 | y=12.514e0.0302x | 0.97 | 2.09[a] | y=11.265e0.0343x | 0.97 | 2.67[b] | y=10.239e0.0348x | 0.95 | 1.58[a] | y=11.681e0.0335x | 0.93 | 3.23[b] |
| A3 | y=13.143e0.028x | 0.96 | 1.90[a] | y=11.861e0.032x | 0.95 | 2.23[b] | y=10.914e0.0327x | 0.90 | 1.93[a] | y=12.39e0.0312x | 0.88 | 3.38[b] |
| C1 | y=11.662e0.0324x | 0.87 | 3.05[a] | y=9.2272e0.041x | 0.85 | 3.83[b] | y=8.551e0.0409x | 0.82 | 3.04[a] | y=11.089e0.0354x | 0.81 | 3.88[b] |
| C2 | y=11.472e0.0333x | 0.94 | 2.74[b] | y=13.411e0.0283x | 0.96 | 2.64a | y=8.0996e0.043x | 0.90 | 2.81[a] | y=10.741e0.0371x | 0.88 | 3.91[b] |
| C3 | y=12.294e0.0305x | 0.91 | 2.43[a] | y=9.7714e0.0391x | 0.88 | 3.25[b] | y=9.1113e0.0392x | 0.84 | 2.77[a] | y=11.739e0.0337x | 0.83 | 3.88[b] |
| E1 | y=12.545e0.0294x | 0.92 | 2.27[a] | y=11.221e0.0337x | 0.92 | 2.61[b] | y=10.415e0.0333x | 0.89 | 2.39[a] | y=11.97e0.032x | 0.89 | 3.06[b] |
| E2 | y=12.395e0.0299x | 0.97 | 1.70[a] | y=11.12e0.0341x | 0.97 | 2.19[b] | y=10.177e0.0347x | 0.95 | 1.73[a] | y=11.825e0.0331x | 0.94 | 3.13[b] |
| E3 | - | - | - | - | - | - | y=10.865e0.0324x | 0.90 | 2.10[a] | y=12.432e0.031x | 0.90 | 3.15[b] |

[a,b]Rank.

terns but were different from the experimental distribution (Figure 7C). Meanwhile, the temperature pattern was different in the S-scenario (Figure 8). The phenomena shown in Figures 7 and 8 were bolstered by the ANOVA result listed in Table 4. Figures 7C and 8C show hotspots at the centre, as expected (Bello-Robles *et al.*, 2018; Bojacá *et al.*, 2009; Ogunlowo *et al.*, 2021). However, the case was not the same in the simulated models due to the differences in the deviation between the experimental and simulation thermal points, as indicated in the RSME values listed in Table 4. Eliminating the deviation ensured a more accurate representation

of the experimental distribution by the models. One method of eliminating the deviation would be through model calibration. Table 5 lists the validation result of all the crop-area thermal points. The regression equations were used to calibrate the respective models in the TRNSYS simulation studio. The outputs of each calibrated model were then used to plot the contour map, as shown in Figures 9 and 10, which show that the calibrated 3D_M models were similar to the experimental contour in both the D and S scenarios. In contrast, the M_M models still exhibited differences in the distribution compared with experimental DLG and SLG.
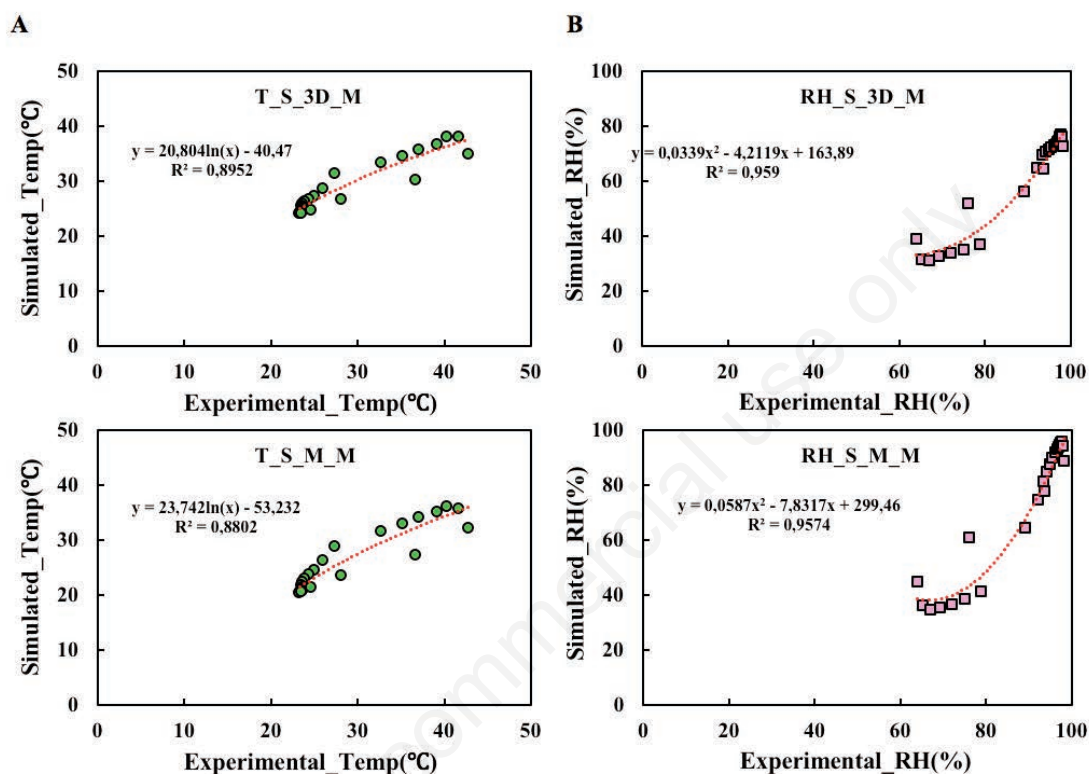


**Figure 6. Plot of the simulated *versus* experimental (A) temperature and (B) relative humidity (RH) in the S-scenario.**
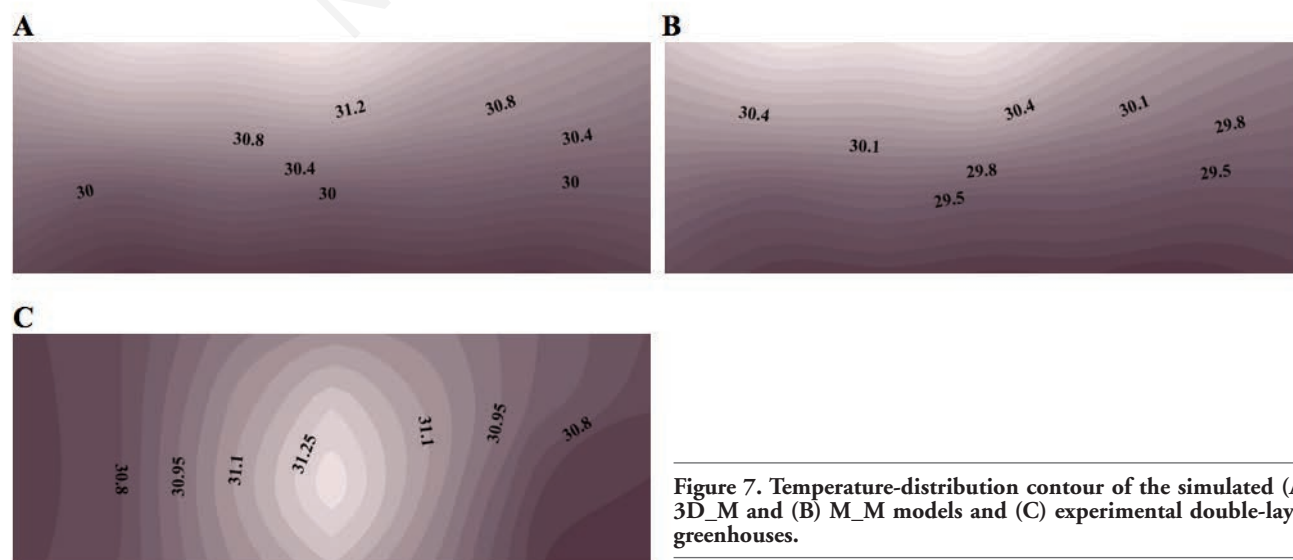


**Figure 7. Temperature-distribution contour of the simulated (A) 3D_M and (B) M_M models and (C) experimental double-layer greenhouses.**
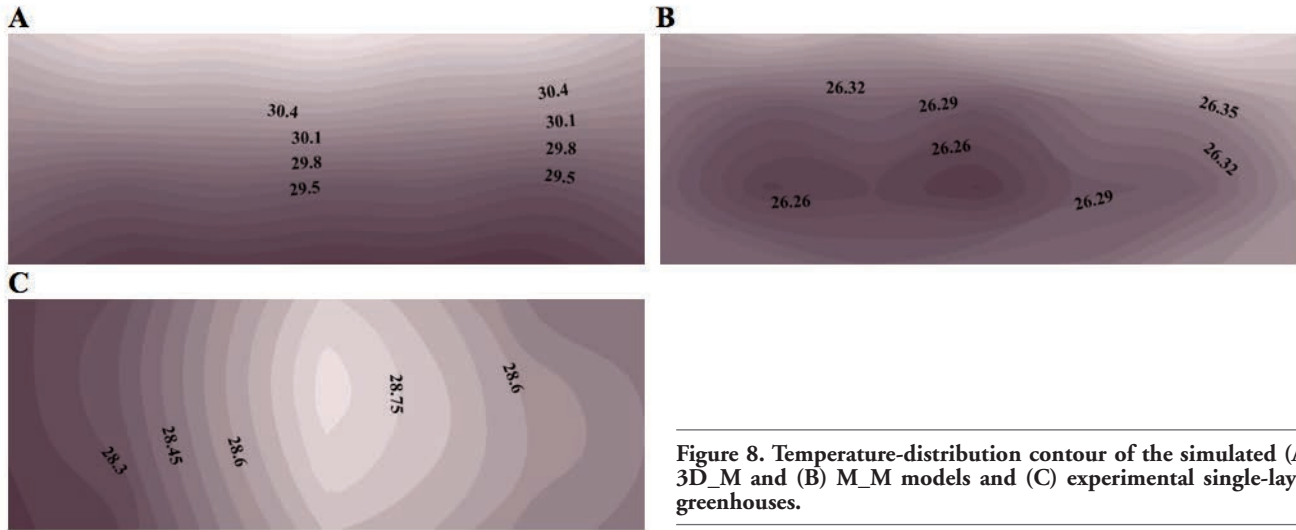
**Figure 8.** Temperature-distribution contour of the simulated (A) 3D_M and (B) M_M models and (C) experimental single-layer greenhouses.
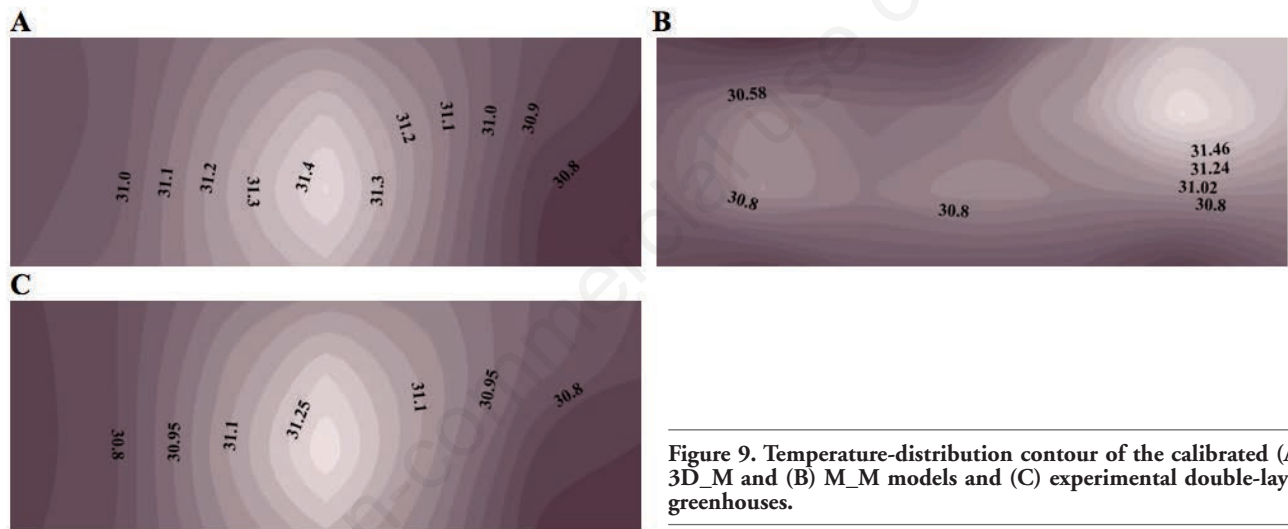


**Figure 9.** Temperature-distribution contour of the calibrated (A) 3D_M and (B) M_M models and (C) experimental double-layer greenhouses.
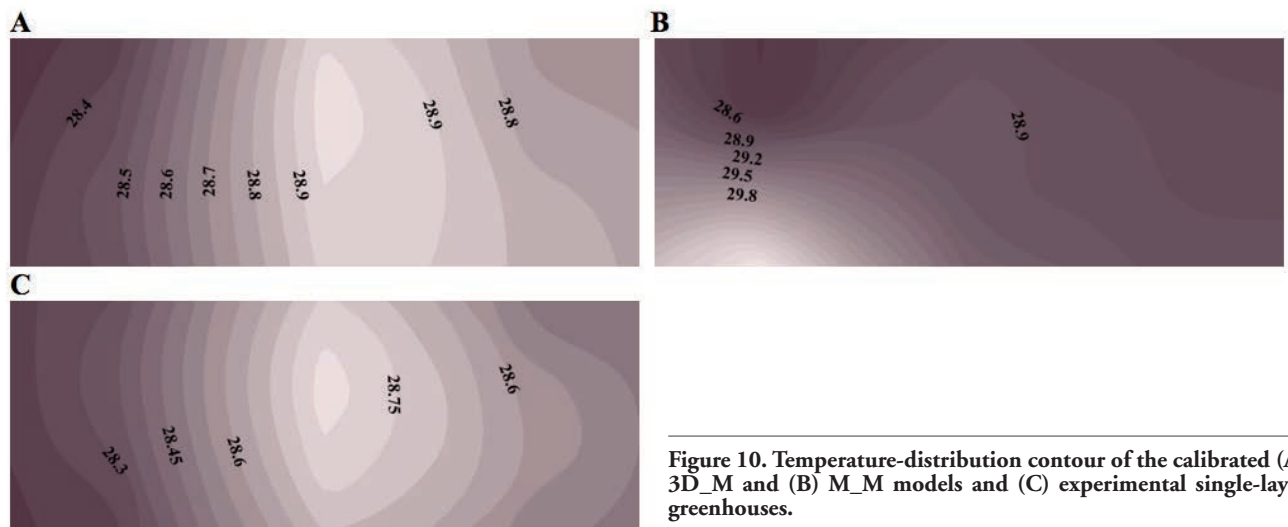


**Figure 10.** Temperature-distribution contour of the calibrated (A) 3D_M and (B) M_M models and (C) experimental single-layer greenhouses.

The import of these results is that to mimic a real-life single- and double-layer greenhouse scenario with a discretised TRNSYS 18 BES model, using a 3D geometry with a massless layer partitioning adjacent air nodes will ensure accurate temperature and RH prediction and their distribution along the crop area.

## Conclusions

Five discretised BES models (D_3D_M, D_3D_W, D_M_M, S_3D_W, and S_M_M) were developed based on the combination of three envelope characteristics (number of layers, geometry mode, and layer type) in TRNSYS 18. The reference factors were the number of layers (D and S), geometry mode (3D and M), and layer type (M and W).

Validation of the models indicated that for the D-scenario models, the $R^2$ value ranged between 0.90 and 0.95, and the RSME value ranged between 2.64°C and 3.75°C in terms of temperature. The values were 0.91%-0.93% and 28.02%-30.32% in terms of RH. In the S-scenario models, the $R^2$ value was between 0.86 and 0.88, and the RSME value was between 2.81°C and 3.91°C for the temperature. Those for RH were between 0.92 and 0.93 and 19.72% and 28.41%, respectively.

There was no significant difference between the D-scenario models and experimental centre-point temperature. Meanwhile, there was no significant difference between the model and experimental centre-point RH for RH, but there were significant differences within the models. Significant differences were also observed between the models and experimental centre-point temperatures and RHs in the S-scenario models.

For the double- and single-layer scenarios, the 3D geometry with a massless layer demonstrated a similar distribution with their corresponding experimental greenhouses.

## References

Akpenpuun T. D., Na W.H., Ogunlowo Q.O., Rabiu A., Adesanya M.A., Addae K.S., Kim T.H., Lee H.W. 2021. Effect of greenhouse cladding materials and thermal screen configuration on heating energy and strawberry (Fragaria Ananassa Var. 'Seolhyang') yield in winter. Agron. 11:1-23.

Akpenpuun T. D., Na W.H., Ogunlowo Q.O., Rabiu A., Adesanya M.A., Addae K.S., Kim T.H., Lee H.W. 2021. Effect of glazing configuration as an energy-saving strategy in naturally ventilated greenhouses for strawberry (Seolhyang Sp.) cultivation. J. Agr. Eng. 52:1-24.

Akpenpuun T.D., Ogunlowo Q.O., Rabiu A., Adesanya M.A., Na W.H., Omobowale M.O., Mijinyawa Y., Lee H.W. 2022. Building energy simulation model application to greenhouse microclimate, covering material and thermal blanket modelling: a review. Niger J. Techn. Dev. 19:3851-6.

Asa'd O., Ugursal V.I., Ben-Abdallah N. 2019. Investigation of the energetic performance of an attached solar greenhouse through monitoring and simulation. Energ. Sustain. Dev. 53:15-29.

Baglivo C., Mazzeo D., Panico S., Bonuso S., Matera N., Congedo P.M., Oliveti G. 2020. Complete greenhouse dynamic simulation tool to assess the crop thermal well-being and energy needs. Appl. Therm. Eng. 179:115698.

Bello-robles J.C., Ruiz-leon J., Begovich O., Ruiz J., Quetziquel R. 2018. Modeling of the temperature distribution of a greenhouse using finite element differential neural networks. Kybernetika. 54:1033-48.

Blachowski W. 2021. A guide to model calibration. Wunderman Thompson Technology Blog. Available from: https://wttech.blog/blog/2021/a-guide-to-model-calibration/

Bojacá C.R., Gil R., Gómez S., Cooman A., Schrevens E. 2009. Analysis of greenhouse air temperature distribution using geostatistical methods. Trans. ASABE. 52:957-68.

Boulard T., Fatnassi H., Majdoubi H., Bouirden L. 2008. Airflow and microclimate patterns in a one-hectare canary type greenhouse: an experimental and CFD assisted study. Acta Hortic. 801:837-45.

Cesar T.Q.Z., Leal P.A.M., Branquinho O.C., Felipe A.M.M. 2021. Wireless sensor network to identify the reduction of meteorological gradients in greenhouse in subtropical conditions. J. Agr. Eng. 52:1-8.

Choab N., Allouhi A., El Maakoul A., Kousksou T., Saadeddine S., Jamil A. 2021. Effect of greenhouse design parameters on the heating and cooling requirement of greenhouses in moroccan climatic conditions. IEEE Access 9:2986-3003.

Coastalwiki. 2020. Definition of model calibration: model calibration. Available from: http://www.coastalwiki.org/wiki/Model_calibration#:~:text=Model calibration is the process,-Fit or Cost Function

Glen S. 2019. Comparing model evaluation techniques part 1: statistical tools & tests. Data Science Central. Available from: https://www.datasciencecentral.com/comparing-model-evaluation-techniques/

Gupta R. 2019. An introduction to discretization techniques for data scientists. Towards Data Science. Available from: https://towardsdatascience.com/an-introduction-to-discretization-in-data-science-55ef8c9775a2

Hamad H., Al-smadi A., Ijjeh A.. 2008. Graphical model validation methods for analog and mixed- signal electronic circuits design. Proc. Inter Conf. Micoelectron. 353-6.

Klein S.A. 2012. Trnsys, a transient system simulation program; solar energy laboratory. University of Wisconsin-Madison, Madison, WI, USA.

Laghmich N., Ramoni Z., Lapisa R. Draoui A. 2022. Numerical analysis of horizontal temperature distribution in large buildings by thermo-aeraulic zonal approach. Build Simul. 15:99-115.

Lamrani M.A., Boulard T., Roy J.C., Jaffrin A. 2001. Airflows and temperature patterns induced in a confined greenhouse. J. Agr. Eng. Res. 8:75-88.

Mazzeo D., Matera N., Cornaro C., Oliveti G., Romagnoni P., De Santoli L. 2020. EnergyPlus, IDA ICE and TRNSYS predictive simulation accuracy for building thermal behaviour evaluation by using an experimental campaign in solar test boxes with and without a PCM module. Energ. Build. 212:109812.

Ogunlowo Q.O., Akpenpuun T.D., Na W.H., Rabiu A., Adesanya M.A., Addae K.S., Kim H.T., Lee H.W. 2021. Analysis of heat and mass distribution in a single- and multi-span greenhouse microclimate. J. Agric. 11:891.

Ogunlowo Q.O., Olaoye J.O. 2017. Development and performance evaluation of a guided horizontal conveyor rice harvester. Agrosearch 17:66-88.

Rabiu A., Na W.H, Akpenpuun T.D., Rasheed A., Adesanya M.A, Ogunlowo Q.O., Kim H.T., Lee H.W. 2022. Determination of overall heat transfer coefficient for greenhouse energy-saving screen using Trnsys and Hotbox. Biosys. Eng. 217:83-101.

Rafiq A., Na W.H, Rasheed A., Kim H.T., Lee H.W. 2019. Determination of thermal radiation emissivity and absorptivity of thermal screens for greenhouse. Protect. Hortic. Plant Factory. 28:311-21.

Rafiq A., Na W.H., Rasheed A., Lee J.W., Kim H.T., Lee H.W. 2021. Measurement of longwave radiative properties of energy-saving greenhouse screens. J. Agricult. Engine. LII:1209.

Rasheed A., Kwak C.S., Na W.H., Lee J.W., Kim H.T., Lee H.W. 2020. Development of a building energy simulation model for control of multi-span greenhouse microclimate. Agron. 10:1236.

Rasheed A., Lee J.W., Lee H.W. 2017. Development of a model to calculate the overall heat transfer coefficient of greenhouse covers. Span. J. Agric. Res. 15:e0208.

Rasheed A., Lee J.W., Lee H.W. 2018. Development and optimization of a building energy simulation model to study the effect of greenhouse design parameters. Energies 11:2001.

Rasheed A., Na W.H, Lee J.W., Kim H.T., Lee H.W. 2019. Optimization of greenhouse thermal screens for maximized energy conservation. Energies 12:3592.

Sanft R., Walter A. 2020. Exploring mathematical modeling in biology through case studies and experimental activities. Elsevier Inc., Amsterdam, The Netherlands, pp. 154-155.

Shamshiri R. 2007. Principles of greenhouse control engineering: theories and concepts. Inst. Adv. Tech. University of Putra, Malaysia.

Sunmin K. 2021. Water engineering modelling and mathematics tools. Elsevier Inc., Amsterdam, The Netherlands, pp. 377.

TRANSSOLAR Energietechnik. 2017. Multizone building modeling with Type56 and TRNBuild. Trnsys 18:49-50.

Villagrán E.A., Romero E.J.B., Bojacá C.R. 2019. Transient CFD analysis of the natural ventilation of three types of greenhouses used for agricultural production in a tropical mountain climate. Biosys. Eng. 188:288-304.

Ward R., Choudhary R., Cundy C., Johnson G., Mcrobie A. 2015. Simulation of plants in buildings; incorporating plant-air interactions in building energy simulation. pp. 2256-2263 in Proc. 14th Intern Conf IBPSA - Building Simulation.

Zhao Y., Teitel M., Barak M. 2001. Vertical temperature and humidity gradients in a naturally ventilated greenhouse. J. Agr. Eng. Res. 78:431-6.